Boltzmann rovibrational collisional coarse-grained model for internal energy excitation and dissociation in hypersonic flows

A. Munafò,[1,*] M. Panesi,[2,†] and T. E. Magin[1,‡]

[1]*Aeronautics and Aerospace Department, von Karman Institute for Fluid Dynamics, Chaussée de Waterloo 72, 1640 Rhode-Saint-Genèse, Belgium*

[2]*Department of Aerospace Engineering, Talbot Laboratory, University of Illinois at Urbana-Champaign, 104 South Wright Street, Urbana, Illinois 61801, USA*

(Received 21 August 2013; revised manuscript received 29 October 2013; published 5 February 2014)

A Boltzmann rovibrational collisional coarse-grained model is proposed to reduce a detailed kinetic mechanism database developed at NASA Ames Research Center for internal energy transfer and dissociation in N_2-N interactions. The coarse-grained model is constructed by lumping the rovibrational energy levels of the N_2 molecule into energy bins. The population of the levels within each bin is assumed to follow a Boltzmann distribution at the local translational temperature. Excitation and dissociation rate coefficients for the energy bins are obtained by averaging the elementary rate coefficients. The energy bins are treated as separate species, thus allowing for non-Boltzmann distributions of their populations. The proposed coarse-grained model is applied to the study of nonequilibrium flows behind normal shock waves and within converging-diverging nozzles. In both cases, the flow is assumed inviscid and steady. Computational results are compared with those obtained by direct solution of the master equation for the rovibrational collisional model and a more conventional multitemperature model. It is found that the proposed coarse-grained model is able to accurately resolve the nonequilibrium dynamics of internal energy excitation and dissociation-recombination processes with only 20 energy bins. Furthermore, the proposed coarse-grained model provides a superior description of the nonequilibrium phenomena occurring in shock heated and nozzle flows when compared with the conventional multitemperature models.

DOI: 10.1103/PhysRevE.89.023001 PACS number(s): 47.70.Nd, 47.40.Ki, 47.60.Kz, 82.20.Rp

I. INTRODUCTION

Hypersonic aerothermodynamics finds its chief application in the description of the flow surrounding spacecraft entering planetary atmospheres [1–3]. The correct modeling of the physicochemical phenomena occurring in hypersonic flows is important for the design of heat shields of space vehicles and for a correct interpretation of experimental measurements in high-enthalpy wind tunnels.

Nonequilibrium effects occur as a result of the finite-rate nature of collisional and radiative processes. The theoretical framework for their description depends on the time scales of the physical processes of interest [4]. When the Knudsen number is sufficiently small, collisions dominate the convective transport and the translational velocity of the gas species are close to equilibrium (Maxwell-Boltzmann distribution function) [5,6]. A hydrodynamic description based on the Navier-Stokes equations can be adopted to determine flow quantities such as velocity and chemical composition, and transport fluxes such as heat flux and stress tensor [7–10]. The inclusion of the internal structure of the gas species (e.g., rotational and vibrational energy levels of molecules) makes the description more complex as the distribution function of the internal energy may deviate from local equilibrium. This situation is found when the elementary processes (such as dissociation and internal energy excitation) occur at the same time scales of the flow often encountered behind shock waves [11–13] and within converging-diverging nozzles [14–17]. The non-Boltzmann character of the internal energy distribution function can have a significant impact on the dynamics of internal energy excitation and dissociation-recombination processes [18]. In the case of the flow inside nozzles in high-enthalpy wind tunnels, nonequilibrium effects can affect the gas outlet conditions, which in turn have an important impact on the outcome of the experimental observations. For example, the shock standoff distance and the pressure distribution over a test sample placed at the nozzle outlet are strongly influenced by the chemical composition and the degree of excitation of internal energy of the test gas [1]. Similar considerations also apply to the description of the dissociating flow occurring behind shock waves developed in front of space vehicles during a planetary entry.

Multitemperature models [1,19,20] have been proposed to model nonequilibrium effects. In these models, the population of each internal energy mode (rotational, vibrational, or electronic) follows a Boltzmann distribution at its own temperature (e.g., rotational, vibrational, and electronic temperatures). To calculate these temperatures and the energy exchanged between all the energy modes, conservation equations for the internal energy modes in thermal nonequilibrium are added to the set of conservation equations for mass, momentum, and total energy. Multitemperature models are easy to implement and have been used extensively in multidimensional flow codes due to their computational efficiency [21–23]. However, since in hypersonic flows the internal energy level populations may significantly depart from Boltzmann distributions, their use is justified only in the case of small departure from equilibrium [24].

Collisional models [14,15,25–41] represent a valid alternative to multitemperature models as they exhibit a wider spectrum of applicability. Each internal energy level is treated

*munafo@vki.ac.be
†Corresponding author: mpanesi@illinois.edu
‡magin@vki.ac.be

as a separate pseudospecies, thus allowing for the modeling of non-Boltzmann population distributions. The higher accuracy and flexibility obtained with the collisional models is counterbalanced by a higher computational cost due the drastic increase in the number of governing equations to be solved and the complexity of the chemical mechanism considered. Moreover, in order to obtain the numerical values of cross sections and rate coefficients for each elementary process, complex and lengthy quantum-chemistry calculations are usually required. For these reasons, the use of collisional models in computational fluid dynamics (CFD) applications has become feasible only recently, due to the advances in computational resources [42–47]. Even in that case, however, the computational time required is still high compared to multitemperature models.

A possible approach to the reduction of the mathematical complexity and the computational cost is coarsening the resolution of the dynamics of the internal energy levels [14,48–53]. This is motivated by the fact that, in CFD applications, one is more interested in the correct prediction of the dynamics of flow quantities and transport fluxes at the wall than resolving the finest details of the internal energy distribution function. In this context, vibrational collisional (VC) models [14,15,31,52] have been proposed assuming that the rotational energy mode is in equilibrium with the translational energy mode.

The purpose of this paper is the development of a Boltzmann rovibrational collisional (BRVC) coarse-grained model for an accurate description of the internal energy excitation and dissociation for the $N_2(^1\Sigma_g{}^+)$-$N(^4S_u)$ system in hypersonic flows. This coarse-grained model is constructed by lumping the rovibrational energy levels of the N_2 molecule into energy bins. A bin collisional model is then derived by assuming that the population of the levels within each bin follows a Boltzmann distribution at the local translational temperature. A similar model has been previously proposed based on a uniform distribution [the Boltzmann uniform rovibrational collisional (URVC) coarse-grained model] [49]. The latter does not allow for retrieving the equilibrium state (chemical composition and energy distribution) and the Boltzmann model is developed here in order to overcome this problem. The BRVC model is based on the *ab initio* database developed by the Computational Quantum Chemistry Group at NASA Ames Research Center [25–27]. This database provides rate coefficients for the rovibrational excitation and dissociation of the ground electronic state of the nitrogen molecule $N_2(^1\Sigma_g{}^+)$ colliding with a nitrogen atom in its ground electronic state $N(^4S_u)$. The coarse-grained model is applied to the modeling of the nonequilibrium flows behind normal shock waves and within converging-diverging nozzles. The modeling of nozzle flows could not be achieved with the URVC model [49] in view of the difficulty of retrieving the equilibrium state (usually assumed in the nozzle reservoir). In all the cases, the flow is considered inviscid, quasi-one-dimensional, and steady. The reason justifying these simplifying assumptions is twofold. First, for one-dimensional and inviscid flows, it is possible to obtain numerical solutions for the rovibrational collisional model with reasonable computational effort. This allows for a direct quantification of the degree of approximation introduced by the coarse-grained model. Second, the assumptions introduced allow for a description of the main features of internal energy excitation and dissociation-recombination processes characterizing hypersonic flows.

The paper is organized as follows. Section II describes the Boltzmann coarse-grained model developed for the reduction of the NASA Ames database together with the flow governing equations. The numerical methods applied to the analysis of the flows under investigation are explained in Sec. III. Computational results are analyzed and discussed in Sec. IV. Finally, the findings are outlined in Sec. V.

II. PHYSICAL MODELING

This section describes the coarse-grained modeling strategy applied to the analysis of hypersonic flows in compressing and expanding environments. First, the main features of the NASA Ames database, describing the dynamics of the $N_2(^1\Sigma_g{}^+)$-$N(^4S_u)$ interactions, are briefly summarized. Then, the steps needed for the development of the BRVC model are discussed in detail. Finally, the governing equations for inviscid and quasi-one-dimensional nonequilibrium flows are prescribed.

A. The NASA Ames database for the $N_2(^1\Sigma_g{}^+)$-$N(^4S_u)$ system

The NASA Ames database [25–27] comprises a complete and self-consistent set of thermodynamic and kinetic data needed to describe the elementary state-to-state kinetics of $N_2(^1\Sigma_g{}^+)$-$N(^4S_u)$ and $N_2(^1\Sigma_g{}^+)$-$N_2(^1\Sigma_g{}^+)$ interactions. While the analysis carried out in this work is restricted to the study of the $N_2(^1\Sigma_g{}^+)$-$N(^4S_u)$ interaction, an ongoing effort addresses the study of the dynamics of the $N_2(^1\Sigma_g{}^+)$-$N_2(^1\Sigma_g{}^+)$ system [54].

The number of rovibrational energy levels $N_2(v, J)$ of the ground electronic state of the N_2 molecule is 9390, where the indices v and J stand for the vibrational and rotational quantum numbers, respectively. Most of these rovibrational levels (7421) are bound. This means that their energy is lower than the dissociation energy relative to the $(v = 0,\ J = 0)$ level, equal to 9.75 eV. The remaining levels are predissociated (or quasibound). Thus their energy is higher than the dissociation energy relative to the level $(v = 0,\ J = 0)$, but lower than the J-dependent centrifugal barrier. The numerical values of the rovibrational energy levels have been obtained by applying the Wentzel-Kramer-Brillouin approximation [55], using the potential for $N_2(^1\Sigma_g{}^+)$ developed by Le Roy *et al.* [56].

The bound and predissociated energy levels can be denoted, respectively, by means of the sets I_B and I_P. These satisfy the relations $I_{BP} = I_B \cup I_P$ and $I_B \cap I_P = \emptyset$. For the sake of later convenience, it is useful to sort the energy levels according to increasing energy and denoting them by means of a global index i. The values of the energy and degeneracy of the level $i \in I_{BP}$ are indicated by the symbols E_i and g_i, respectively.

More than 20 million reactions are considered: (i) collisional dissociation from bound and predissociated states:

$$N_2(i) + N \underset{k_i^R(T)}{\overset{k_i^D(T)}{\rightleftarrows}} N + N + N, \quad i \in I_{BP}; \tag{1}$$

(ii) predissociation (or tunneling) of predissociated states:

$$\mathrm{N}_2(i) \underset{k_i^{IP}(T)}{\overset{k_i^{P}(T)}{\rightleftarrows}} \mathrm{N} + \mathrm{N}, \quad i \in I_P; \tag{2}$$

and (iii) collisional excitation among bound and predissociated states:

$$\mathrm{N}_2(i) + \mathrm{N} \underset{k^E_{j\to i}(T)}{\overset{k^E_{i\to j}(T)}{\rightleftarrows}} \mathrm{N}_2(j) + \mathrm{N}, \quad i < j;\ i,j \in I_{BP}. \tag{3}$$

In the present work, predissociation is not accounted for. The rate coefficients for collisional dissociation and excitation [$k_i^D(T)$ and $k^E_{i\to j}(T)$, with $i < j$, respectively] have been computed by integrating over a Maxwell-Boltzmann distribution function for the translational energy the cross-section values obtained by means of the quasi-classical-trajectory method [25–27]. Rate coefficients are available at nine values of temperature between 7500 and 50 000 K.

The (exothermic) rate coefficients for recombination and deexcitation processes [$k_i^R(T)$ and $k^E_{j\to i}(T)$, with $i < j$, respectively] are computed based on microreversibility [57,58]:

$$\frac{k_i^R(T)}{k_i^D(T)} = \frac{g_i Q^{\mathrm{tr}}_{\mathrm{N}_2}(T)}{\left[g_{\mathrm{N}} Q^{\mathrm{tr}}_{\mathrm{N}}(T)\right]^2} \exp\left(\frac{2E_{\mathrm{N}} - E_i}{k_b T}\right), \quad i \in I_{BP}, \tag{4}$$

$$\frac{k^E_{j\to i}(T)}{k^E_{i\to j}(T)} = \frac{g_i}{g_j} \exp\left(\frac{E_j - E_i}{k_b T}\right), \quad i < j;\ i,j \in I_{BP}, \tag{5}$$

where k_b is Boltzmann's constant. The degeneracy of the N atom in its ground electronic state g_{N} in Eq. (4) is equal to 12. The quantity E_{N} represents the formation energy of the N atom. The translational partition functions of N and N_2 are:

$$Q^{\mathrm{tr}}_{\mathrm{N}}(T) = \left(\frac{2\pi m_{\mathrm{N}} k_b T}{h_p^2}\right)^{3/2}, \quad Q^{\mathrm{tr}}_{\mathrm{N}_2}(T) = \left(\frac{2\pi m_{\mathrm{N}_2} k_b T}{h_p^2}\right)^{3/2}, \tag{6}$$

where h_p is Planck's constant and m_{N} and m_{N_2} are the masses of N and N_2, respectively. The production rates for N and for the internal energy levels of N_2 due to collisional dissociation and excitation (and the related reverse exothermic processes) are computed based on the zeroth-order reaction rate theory [57,58]:

$$\omega_{\mathrm{N}} = 2 m_{\mathrm{N}} n_{\mathrm{N}} \sum_{i \in I_{BP}} \left[n_i k_i^D(T) - n_{\mathrm{N}}^2 k_i^R(T)\right], \tag{7}$$

$$\begin{aligned}\omega_i = {} & -m_{\mathrm{N}_2} n_{\mathrm{N}} \left[n_i k_i^D(T) - n_{\mathrm{N}}^2 k_i^R(T)\right] \\ & + m_{\mathrm{N}_2} n_{\mathrm{N}} \sum_{\substack{j \in I_{BP} \\ j < i}} \left[n_j k^E_{j\to i}(T) - n_i k^E_{i\to j}(T)\right] \\ & - m_{\mathrm{N}_2} n_{\mathrm{N}} \sum_{\substack{j \in I_{BP} \\ j > i}} \left[n_i k^E_{i\to j}(T) - n_j k^E_{j\to i}(T)\right], \quad i \in I_{BP},\end{aligned} \tag{8}$$

where n_{N} and n_i are the number densities of N and the internal energy level i of N_2, respectively.

The set of thermodynamic and state-to-state kinetics data described in this section constitutes a rovibrational collisional (RVC) model [18]. This has been applied to study rovibrational energy transfer and dissociation in zero- [18] and one-dimensional [59] systems. The RVC model provides the basis for the construction of the BRVC model, which is explained in detail in Sec. II B.

B. Boltzmann rovibrational collisional model

The BRVC model is constructed based on the RVC model (described in Sec. II A) by lumping the energy levels of N_2 into energy bins. The construction of the proposed coarse-grained model goes as follows.

First, the whole internal energy ladder of N_2 is divided in two parts: one for the bound levels and the other for the predissociated levels. Second, both regions are evenly subdivided with spacing:

$$\Delta E_B = 2E_{\mathrm{N}}/N_B, \quad \Delta E_P = (E_\star - 2E_{\mathrm{N}})/N_P, \tag{9}$$

where the number of energy bins for the bound and predissociated regions (N_B and N_P, respectively) is a free parameter and such that $N_{BP} = N_B + N_P$ (where N_{BP} is the total number of energy bins). The quantity $E_\star$ represents the energy of the last energy level. The next step consists in the construction of a map between energy bins and energy levels in order to associate the energy level i with the energy bin k it belongs to:

$$\mathcal{B}(i) = \begin{cases} \lfloor E_i/\Delta E_B \rfloor + 1, & i \in I_B \\ \lfloor (E_i - 2E_{\mathrm{N}})/\Delta E_P \rfloor + N_B + 1, & i \in I_P, \end{cases} \tag{10}$$

where $\mathcal{B}$ denotes bin and the symbol $\lfloor\,\rfloor$ stands for the floor function. It is important to mention that the procedure discussed here can lead to the formation of empty bins, which are then removed from the model. For the sake of later convenience it is useful to introduce the sets K_B, K_P, and K_{BP}, storing, respectively, the indices for the energy bins associated with the bound, predissociated, and both the bound and predissociated levels (satisfying the relations $K_{BP} = K_B \cup K_P$ and $K_B \cap K_P = \emptyset$) and the set I_k storing the energy levels belonging to the energy bin k:

$$I_k = \{i \in I_{BP} | \mathcal{B}(i) = k\}, \quad k \in K_{BP}. \tag{11}$$

Based on the subdivision into energy bins constructed through Eqs. (9)–(11), it is possible to write the energy E_i of the level i within the energy bin k based on the energy $\tilde{E}_k$ of the first level within the same bin as:

$$E_i = \tilde{E}_k + \Delta\tilde{E}_k(i), \quad i \in I_k;\ k \in K_{BP}. \tag{12}$$

The bin energy $\tilde{E}_k$ and the $\Delta\tilde{E}_k(i)$ energy contribution are the equivalent of the vibrational and rotational energy, respectively, in a VC model [14]. The population of the rovibrational energy levels grouped in the energy bins can be easily obtained once the bin distribution is specified. In this work, it is assumed that the population of the energy levels within each bin follows a Boltzmann distribution at the local translational temperature T:

$$\frac{n_i}{\tilde{n}_k} = \frac{g_i}{\tilde{Q}_k(T)} \exp\left(-\frac{\Delta\tilde{E}_k(i)}{k_b T}\right), \quad i \in I_k;\ k \in K_{BP}, \tag{13}$$

where the number density $\tilde{n}_k$ and the partition function $\tilde{Q}_k(T)$ of the energy bin k in Eq. (13) are defined as:

$$\tilde{n}_k = \sum_{i \in I_k} n_i, \tag{14}$$

$$\tilde{Q}_k(T) = \sum_{i \in I_k} g_i \exp\left(-\frac{\Delta \tilde{E}_k(i)}{k_b T}\right), \quad k \in K_{BP}. \tag{15}$$

The assumption of local equilibrium of the internal levels within each bin is justified by the large reaction rate coefficients for excitation and deexcitation that characterize groups of levels with similar internal energy. This assumption is found to work quite well in the condition of interest to this work, as shown in Sec. IV. Furthermore, increasing the number of energy bins can easily extend the range of validity of this model to stronger nonequilibrium conditions.

Equation (13) holds true in equilibrium conditions. This means that the BRVC model does not introduce modifications, when compared to the RVC model, as far as equilibrium thermodynamic properties are concerned. This was not the case for the URVC model [49]. For the BRVC model, it can be shown that the equilibrium population of the energy bins is given by a Boltzmann distribution:

$$\frac{\tilde{n}_k}{n_{N_2}} = \frac{\tilde{Q}_k(T)\exp\left(-\tilde{E}_k/k_b T\right)}{\sum_{k \in K_{BP}} \tilde{Q}_k(T)\exp\left(-\tilde{E}_k/k_b T\right)}, \quad k \in K_{BP}, \tag{16}$$

where the partition function $\tilde{Q}_k(T)$ of the energy bin k plays the role of a degeneracy. The number density of N_2 in Eq. (16) is computed as $n_{N_2} = \sum_{k \in K_{BP}} \tilde{n}_k$.

1. Bin-averaged rate coefficients

In order to obtain the bin-averaged rate coefficients, Eqs. (7) and (8) are considered and Eq. (8) (providing the mass production rate ω_i for the energy level i) is summed over all the energy levels belonging to the energy bin k (stored in the set I_k). After performing some algebraic manipulations, the mass production terms for N and the energy bin k of N_2 are obtained:

$$\omega_N = 2 m_N n_N \sum_{k \in K_{BP}} \left[\tilde{n}_k \tilde{k}^D_k(T) - n_N^2 \tilde{k}^R_k(T)\right], \tag{17}$$

$$\begin{aligned}\tilde{\omega}_k = &- m_{N_2} n_N \left[\tilde{n}_k \tilde{k}^D_k(T) - n_N^2 \tilde{k}^R_k(T)\right] \\ &+ m_{N_2} n_N \sum_{\substack{l \in K_{BP} \\ l < k}} \left[\tilde{n}_l \tilde{k}^E_{l\to k}(T) - \tilde{n}_k \tilde{k}^E_{k\to l}(T)\right] \\ &- m_{N_2} n_N \sum_{\substack{l \in K_{BP} \\ l > k}} \left[\tilde{n}_k \tilde{k}^E_{k\to l}(T) - \tilde{n}_l \tilde{k}^E_{l\to k}(T)\right], \quad k \in K_{BP}.\end{aligned} \tag{18}$$

The bin-averaged dissociation and excitation rate coefficients [$\tilde{k}^D_k(T)$ and $\tilde{k}^E_{k\to l}(T)$, with $k < l$, respectively] are defined as:

$$\tilde{k}^D_k(T) = \frac{1}{\tilde{Q}_k(T)} \sum_{i \in I_k} g_i \exp\left(-\frac{\Delta \tilde{E}_k(i)}{k_b T}\right) k^D_i(T), \quad k \in K_{BP}, \tag{19}$$

$$\tilde{k}^E_{k\to l}(T) = \frac{1}{\tilde{Q}_k(T)} \sum_{i \in I_k} g_i \exp\left(-\frac{\Delta \tilde{E}_k(i)}{k_b T}\right) \sum_{j \in I_l} k^E_{i\to j}(T), \quad k < l;\ k,l \in K_{BP}, \tag{20}$$

while the rate coefficients for the reverse processes read:

$$\frac{\tilde{k}^R_k(T)}{\tilde{k}^D_k(T)} = \frac{Q^{tr}_{N_2}(T)\tilde{Q}_k(T)}{\left[g_N Q^{tr}_N(T)\right]^2} \exp\left(\frac{2E_N - \tilde{E}_k}{k_b T}\right), \quad k \in K_{BP}, \tag{21}$$

$$\frac{\tilde{k}^E_{l\to k}(T)}{\tilde{k}^E_{k\to l}(T)} = \frac{\tilde{Q}_k(T)}{\tilde{Q}_l(T)} \exp\left(\frac{\tilde{E}_l - \tilde{E}_k}{k_b T}\right), \quad k < l;\ k,l \in K_{BP}. \tag{22}$$

Equations (21) and (22) state that the bin-averaged rate coefficients for the reverse processes can be computed by applying microreversibility to the bin-averaged rate coefficients for the direct processes as opposed to the URVC model [49].

2. Thermodynamic properties

The gas number density n is obtained by summing the contributions of N and N_2:

$$n = n_N + n_{N_2}, \tag{23}$$

and the static pressure is computed based on Dalton's law $p = n_N k_b T + n_{N_2} k_b T$. The gas thermal energy density ρe is obtained by summing the contributions from the translational energy of N and N_2, the formation energy of N, and the internal energy levels of N_2:

$$\rho e = \frac{3}{2} n_N k_b T + \frac{3}{2} n_{N_2} k_b T + n_N E_N + \sum_{i \in I_{BP}} n_i E_i. \tag{24}$$

Using Eqs. (13)–(15) it is possible to write the last term in Eq. (24) (associated with the internal energy levels of N_2) in the following form:

$$\sum_{i \in I_{BP}} n_i E_i = \sum_{k \in K_{BP}} \tilde{n}_k \tilde{E}_k + \sum_{k \in K_{BP}} \tilde{n}_k k_b T^2 \frac{\partial \ln \tilde{Q}_k(T)}{\partial T}. \tag{25}$$

The first and second contributions in Eq. (25) are the macroscopic bin energy density and the macroscopic intrabin energy density, respectively. These are the equivalent of the macroscopic vibrational and rotational energy densities, respectively, in a VC model [14]. The gas total energy density ρE is obtained by adding the kinetic energy contribution to the gas thermal energy density $\rho E = \rho e + \rho u^2/2$ (with u being the gas velocity and ρ its density $\rho = n_N m_N + n_{N_2} m_{N_2}$). The gas total enthalpy density is computed by adding the static pressure to the total energy density $\rho H = \rho E + p$.

The internal temperature T_{int} is extracted from the computed energy bin population (assumed to be Boltzmann) as postprocessing as follows:

$$\frac{\sum_{k \in I_{BP}} \tilde{n}_k \tilde{E}_k}{n_{N_2}} = \frac{\sum_{k \in I_{BP}} \tilde{Q}_k(T)\tilde{E}_k \exp\left(-\tilde{E}_k/k_b T_{int}\right)}{\sum_{k \in I_{BP}} \tilde{Q}_k(T)\exp\left(-\tilde{E}_k/k_b T_{int}\right)}. \tag{26}$$

C. Governing equations

The governing equations for an inviscid and quasi-one-dimensional nonequilibrium flow within a channel of variable cross-sectional area $A = A(x)$ can be written in conservation law form as [60]:

$$\frac{\partial \mathbf{U}}{\partial t} + \frac{\partial \mathbf{F}}{\partial x} = \mathbf{S}. \tag{27}$$

The vector quantities $\mathbf{U}$, $\mathbf{F}$, and $\mathbf{S}$ appearing in Eq. (27) are the conservative variable, inviscid flux, and source term vectors, respectively. The source term vector $\mathbf{S}$ in Eq. (27) is the sum of two distinct contributions:

$$\mathbf{S} = \mathbf{\Omega} - \frac{d \ln A}{dx}\mathbf{G}, \tag{28}$$

where the vector $\mathbf{\Omega}$ accounts for the collisional processes considered in the proposed BRVC model (see Sec. II B) and the vector $-d \ln A/dx\mathbf{G}$ accounts for the channel cross-sectional area variation [for the case of a normal shock wave $A = \text{const}$ in Eq. (28) and hence $\mathbf{S} = \mathbf{\Omega}$]. The detailed expressions for the vectors $\mathbf{U}$, $\mathbf{F}$, $\mathbf{G}$, and $\mathbf{\Omega}$ in Eqs. (27) and (28) are:

$$\mathbf{U} = [\, \rho_{\mathrm{N}} \;\; \tilde{\rho}_k \;\; \rho u \;\; \rho E \,]^{\mathrm{T}}, \tag{29}$$

$$\mathbf{F} = [\, \rho_{\mathrm{N}} u \;\; \tilde{\rho}_k u \;\; p + \rho u^2 \;\; \rho H u \,]^{\mathrm{T}}, \tag{30}$$

$$\mathbf{G} = [\, \rho_{\mathrm{N}} u \;\; \tilde{\rho}_k u \;\; \rho u^2 \;\; \rho H u \,]^{\mathrm{T}}, \tag{31}$$

$$\mathbf{\Omega} = [\, \omega_{\mathrm{N}} \;\; \tilde{\omega}_k \;\; 0 \;\; 0 \,]^{\mathrm{T}}, \quad k \in K_{BP}, \tag{32}$$

where the partial densities of N and the energy bin k of N_2 are $\rho_{\mathrm{N}} = m_{\mathrm{N}} n_{\mathrm{N}}$ and $\tilde{\rho}_k = \tilde{n}_k m_{\mathrm{N}_2}$, respectively.

III. NUMERICAL METHODS

In the present work, two families of numerical methods are considered. A finite-difference (FD) method is used for the investigation of the nonequilibrium flow behind a normal shock wave and a finite-volume (FV) method is used for computing the nonequilibrium flow within converging-diverging nozzles.

A. Finite-difference method

The inviscid and steady nonequilibrium flow behind a normal shock wave is studied in the shock wave reference frame. In this way, the mathematical problem reduces to an initial-value problem (IVP) for a system of ordinary differential equations (ODEs). Numerical solutions are sought as follows.

The flow governing equations (27) are rewritten under the hypothesis of steady flow and rearranged as a set of ODEs in canonical form [61]:

$$\frac{d\mathbf{P}}{dx} = \mathbf{Q}(\mathbf{P}). \tag{33}$$

In the present work, the vector of working variables $\mathbf{P}$ in Eq. (33) is conveniently set to:

$$\mathbf{P} = [\, y_{\mathrm{N}} \;\; \tilde{y}_k \;\; u \;\; T \,]^{\mathrm{T}}, \quad k \in K_{BP}, \tag{34}$$

where the mass fractions of N and the energy bin k of N_2 are $y_{\mathrm{N}} = \rho_{\mathrm{N}}/\rho$ and $\tilde{y}_k = \tilde{\rho}_k/\rho$, respectively. The vector $\mathbf{Q}(\mathbf{P})$ in Eq. (33) is equal to $(\partial \mathbf{F}/\partial \mathbf{P})^{-1}\mathbf{\Omega}$.

In order to solve the first-order IVP represented by Eq. (33), an initial condition must be provided [61]. This is obtained based on the jump relations expressing the conservation of mass, momentum, and energy fluxes across the shock wave (where it is assumed that the dissociation and excitation are frozen). Notice that the postshock conditions to be used as the initial value for the solution of Eq. (33) depend on the number of energy bins in view of the nonlinear temperature-dependent term of Eq. (25).

Due to the typical stiffness of chemical kinetics problems, Eq. (33) is solved by using the family of backward-differentiation-formula implicit methods [61] as implemented in the LSODE FORTRAN library [62].

B. Finite-volume method

The numerical procedure used for computing the inviscid and nonequilibrium steady flow within nozzles is based on the application of the method of lines [60], i.e. by separating the spatial and temporal discretization. The spatial discretization of Eq. (27) is performed by means of the FV method [60]. Its application leads to the following ODE describing the time evolution of the conservative variable vector of the cell i:

$$\frac{d\mathbf{U}_i}{dt}\Delta x_i + \tilde{\mathbf{F}}_{i+1/2} - \tilde{\mathbf{F}}_{i-1/2} = \mathbf{S}_i \Delta x_i, \tag{35}$$

with the cell volume (length) $\Delta x_i = x_{i+1/2} - x_{i-1/2}$. The numerical inviscid flux $\tilde{\mathbf{F}}_{i+1/2}$ in Eq. (35) is computed by means of Roe's approximate Riemann solver [63]:

$$\tilde{\mathbf{F}}_{i+1/2} = \tfrac{1}{2}[\mathbf{F}(\mathbf{U}_{i+1}) + \mathbf{F}(\mathbf{U}_i)] - \tfrac{1}{2}|\mathbf{A}(\overline{\mathbf{U}})|(\mathbf{U}_{i+1} - \mathbf{U}_i), \tag{36}$$

where $|\mathbf{A}(\overline{\mathbf{U}})| = \mathbf{R}(\overline{\mathbf{U}})|\mathbf{\Lambda}(\overline{\mathbf{U}})|\mathbf{L}(\overline{\mathbf{U}})$ (with $\mathbf{\Lambda}$, $\mathbf{R}$, and $\mathbf{L}$ being, respectively, the eigenvalue, right eigenvector, and left eigenvector matrices associated with the inviscid flux Jacobian matrix $\mathbf{A} = \partial \mathbf{F}/\partial \mathbf{U} = \mathbf{R}\mathbf{\Lambda}\mathbf{L}$ [21,22,60]). The overbar in Eq. (36) indicates that the conservative variables must be evaluated at Roe's averaged state. In the present work, the latter is computed based on the linearization proposed by Prabhu [64].

Once the spatial discretization performed, Eq. (35) is integrated in time by means of the implicit backward-Euler method [60,61]:

$$\frac{\delta \mathbf{U}_i^n}{\Delta t_i}\Delta x_i + \tilde{\mathbf{F}}_{i+1/2}^{n+1} - \tilde{\mathbf{F}}_{i-1/2}^{n+1} = \mathbf{S}_i^{n+1}\Delta x_i, \tag{37}$$

with $\delta \mathbf{U}_i^n = \mathbf{U}_i^{n+1} - \mathbf{U}_i^n$. The local time step Δt_i for the cell i in Eq. (37) is computed based on the Courant-Friedrichs-Lewy number σ as $\Delta t_i = \sigma \Delta x_i/(|u| + c)_i$, with c being the local frozen speed of sound [22]. In order to advance the solution from the time level n to the time level $n+1$, the flux and source terms in Eq. (37) are linearized around the solution at the time level n. In doing this, the source term Jacobian matrix is computed by means of an exact differentiation (in order to enhance stability) while the numerical flux Jacobian matrices are approximated by means of the positive-negative split Jacobian matrices $\mathbf{A}^{\pm} = \mathbf{R}\mathbf{\Lambda}^{\pm}\mathbf{L}$ [60,65]. The final outcome is a block-tridiagonal system to be solved at each time step:

$$\tilde{\mathbf{B}}_{\mathrm{L}\,i}^{\;n}\delta \mathbf{U}_{i-1}^n + \tilde{\mathbf{B}}_{\mathrm{C}\,i}^{\;n}\delta \mathbf{U}_i^n + \tilde{\mathbf{B}}_{\mathrm{R}\,i}^{\;n}\delta \mathbf{U}_{i+1}^n = -\tilde{\mathbf{R}}_i^n. \tag{38}$$

The right-hand-side residual $\tilde{\mathbf{R}}_i$ and the matrices $\tilde{\mathbf{B}}_{\mathrm{L}\,i}$, $\tilde{\mathbf{B}}_{\mathrm{C}\,i}$, and $\tilde{\mathbf{B}}_{\mathrm{R}\,i}$ in Eq. (38) have the following expressions:

$$\tilde{\mathbf{R}}_i = \tilde{\mathbf{F}}_{i+1/2} - \tilde{\mathbf{F}}_{i-1/2} - \mathbf{S}_i \Delta x_i, \tag{39}$$

$$\tilde{\mathbf{B}}_{\mathrm{L}\,i} = -\mathbf{A}^{+}_{i-1}, \tag{40}$$

$$\tilde{\mathbf{B}}_{\mathrm{C}\,i} = \mathbf{I}\frac{\Delta x_i}{\Delta t_i} + |\mathbf{A}_i| - \frac{\partial \mathbf{S}_i}{\partial \mathbf{U}_i}\Delta x_i, \tag{41}$$

$$\tilde{\mathbf{B}}_{\mathrm{R}\,i} = \mathbf{A}^{-}_{i+1}. \tag{42}$$

The symbol $\mathbf{I}$ in Eq. (41) stands for the identity matrix. The algebraic system in Eq. (38) is solved by means of Thomas' algorithm [60] and the solution updated at the time level $n+1$:

$$\mathbf{U}_i^{n+1} = \mathbf{U}_i^n + \delta \mathbf{U}_i^n. \tag{43}$$

This process is continued until steady state is not reached.

The monotone upstream centered schemes for conservation laws approach [66] is considered (with van Albada's slope limiter [67]) in order to achieve second-order accuracy in space. Boundary conditions are applied through ghost cells [60].

IV. COMPUTATIONAL RESULTS

The BRVC model described in Sec. II B has been applied to the investigation of the inviscid and nonequilibrium steady flows behind a normal shock wave and within converging-diverging nozzles. The simulations have been run by using the number of energy bins given in Table I. The number of energy bins associated with the bound levels is about 80% of the total (based on the fact that about 80% of the rovibrational levels are bound). For each case investigated, the results have been compared with those obtained by means of multitemperature (MT) models [1,19] and the RVC model (only for the case of shock waves).

A. Flow behind a normal shock wave

The inviscid flow behind a normal shock wave has been computed by applying the FD method outlined in Sec. III A. Since only $N_2 + N$ collisions are accounted for, the free stream is seeded with 2.8% of N. Table II provides the free stream and postshock equilibrium values for pressure, temperature, and velocity.

Figure 1 shows the evolution behind the shock wave of the temperatures and the N and N_2 mole fractions when using 100 energy bins (BRVC 100). In the region lying between the $x = 0$ and 2.5×10^{-3} m positions, collisions among the gas particles lead to the excitation of internal energy, as can be appreciated from the increase of the internal temperature. Moving further downstream, the excitation process continues with the internal temperature reaching a maximum and then approaching its postshock equilibrium value. At the same time, the dissociation of N_2 starts occurring and becomes significant once the $x = 2.5 \times 10^{-3}$ m location has passed. A first non-negligible part of the dissociation occurs under thermal nonequilibrium conditions [see Fig. 9(b)]. Thermal equilibrium is reached around the location $x = 5 \times 10^{-3}$ m, where more than one-half of N_2 is already dissociated. The remaining part of the dissociation occurs under thermal equilibrium conditions. Notice that, unlike with what is usually observed when using multitemperature models [19], the internal temperature always remains lower than the translational temperature.

A more accurate description of the energy transfer and dissociation processes occurring in the postshock relaxation area can be obtained from the analysis of the energy bin

TABLE I. Number of energy bins (BRVC model).

No.	N_{BP}	N_B	N_P
1	2	1	1
2	5	4	1
3	10	8	2
4	20	16	4
5	30	24	6
6	40	32	8
7	50	40	10
8	75	60	15
9	100	80	20

TABLE II. Free stream and postshock equilibrium conditions.

Condition	p (Pa)	T (K)	u (m/s)
free stream	13.33	300	10 000
postshock equilibrium	13 695	11 420	730

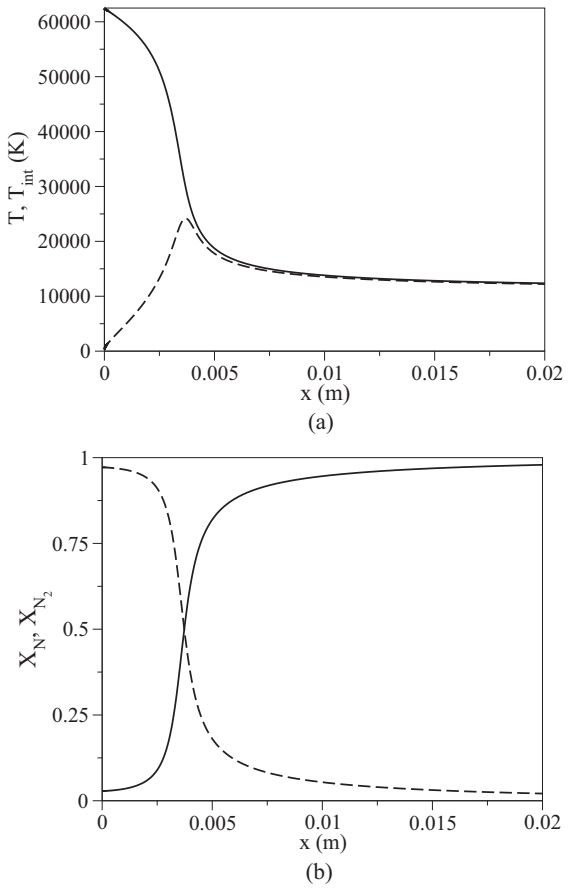

FIG. 1. Temperature and mole fraction evolution behind the shock wave (BRVC 100): (a) T (solid line) and T_{int} (dashed line) and (b) X_{N} (solid line) and $X_{\mathrm{N_2}}$ (dashed line).

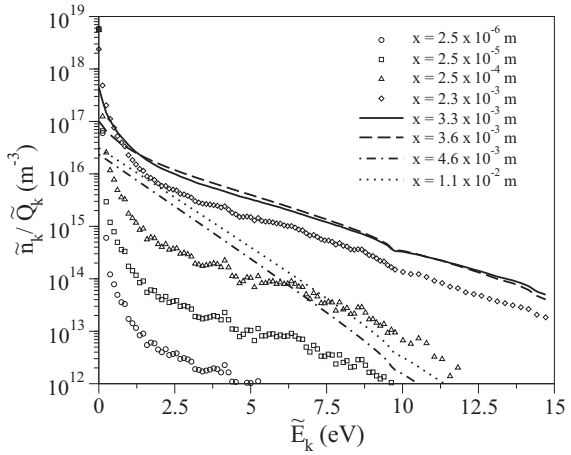

FIG. 2. Population evolution behind the shock wave (BRVC 100).

dynamics. This can be observed in Fig. 2, which shows the energy bin distribution at different locations (with the corresponding values for the N mole fraction and temperatures provided in Table III). The initial part of the excitation occurs through sequences of strongly-non-Boltzmann distributions. After this phase, where multiquantum transitions lead to an increase of the population of high-lying energy bins, the population distribution becomes almost Boltzmann, with the exception of the region close to the ground state. The dissociation initially occurs under thermal nonequilibrium conditions. Deviations from a Boltzmann distribution (around the ground state) are still noticeable at the location $x = 3.6 \times 10^{-3}$ m, where more than 40% of N_2 has already undergone dissociation. The rest of the dissociation occurs through sequences of Boltzmann distributions.

Figure 3 compares the BRVC model solution with those obtained by means of the RVC and MT models. The MT model used was proposed by Park [19] and it accounts for three distinct temperatures (translational, rotational, and vibrational). In this model, the rotational translational and vibrational translational energy transfers are described by using the Parker [68] and the Landau-Teller [1] models, respectively. The comparison in Fig. 3 shows that the BRVC model solution is in good agreement with that of the RVC model, even if the dissociation is slightly faster. On the contrary, the MT model drastically overestimates the dissociation rate. In particular, it is possible to observe a drastic drop in the translational temperature preceding the onset of dissociation. The source

TABLE III. Position, N mole fraction, and temperatures behind the shock (BRVC 100 model).

x (m)	X_N	T (K)	T_{int} (K)
2.5×10^{-6}	2.8×10^{-2}	62 413	377
2.5×10^{-5}	2.8×10^{-2}	62 353	643
2.5×10^{-4}	2.9×10^{-2}	61 755	1 846
2.3×10^{-3}	7.5×10^{-2}	52 655	11 948
3.3×10^{-3}	2.4×10^{-1}	39 649	20 778
3.6×10^{-3}	4.2×10^{-1}	31 975	23 952
4.6×10^{-3}	7.7×10^{-1}	20 367	19 168
1.1×10^{-2}	9.6×10^{-1}	13 431	13 197

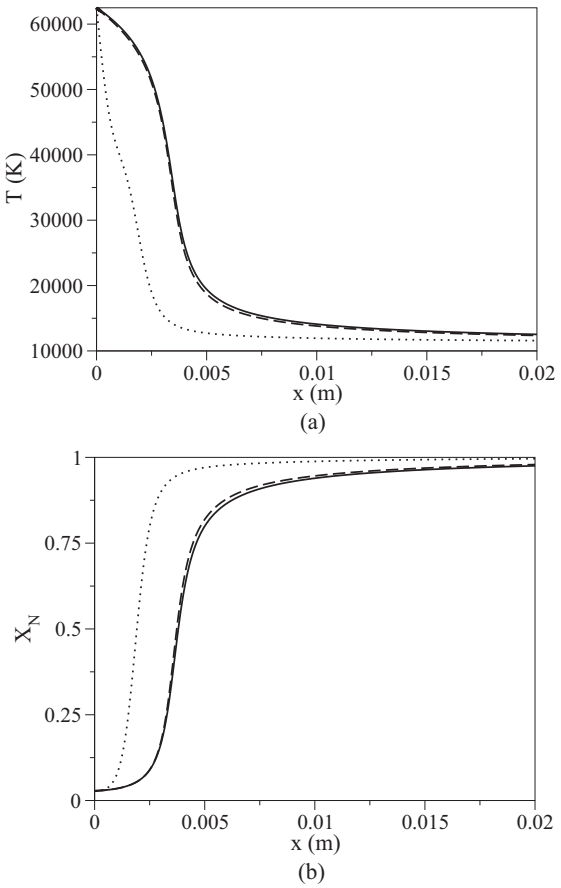

FIG. 3. Comparison between the BRVC 100 (dashed line), RVC (solid line), and MT (dotted line) models for the (a) translational temperature and (b) N mole fraction evolution behind the shock wave.

of this problem could be traced back to the inadequacy of the Parker model [68] in predicting rotational relaxation at high temperatures.

In order to promote a better understanding of the differences observed in Fig. 3 between the BRVC and RVC model solutions, the N mass production term ω_N [given in Eq. (7)] and the chemistry-internal energy and translational-internal energy transfer terms (Ω^{CI} and Ω^{TI}, respectively) are shown in Fig. 4 for both models. The Ω^{CI} and Ω^{TI} energy transfer terms are defined as:

$$\Omega^{CI} = -n_N \sum_{i \in I_{BP}} E_i \left[n_i k_i^D(T) - n_N^2 k_i^R(T) \right], \tag{44}$$

$$\Omega^{TI} = n_N \sum_{\substack{i,j \in I_{BP} \\ j<i}} E_i \left[n_j k_{j\to i}^E(T) - n_i k_{i\to j}^E(T) \right] - n_N \sum_{\substack{i,j \in I_{BP} \\ j>i}} E_i \left[n_i k_{i\to j}^E(T) - n_j k_{j\to i}^E(T) \right]. \tag{45}$$

The results in Fig. 4 show that the BRVC model describes the translational-internal energy transfer with great accuracy. In contrast, ω_N (Ω^{CI}) exhibits a more pronounced maximum (minimum). This is consistent with the behavior observed in Fig. 3, where the dissociation rate is slightly overestimated by the BRVC model.

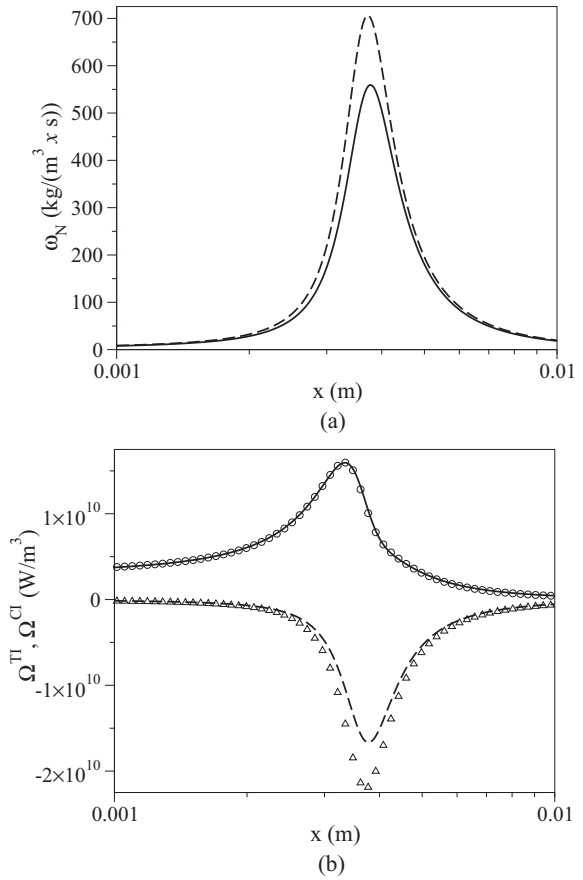

FIG. 4. Comparison between the BRVC 100 and RVC models for (a) the N mass production term and (b) the chemistry-internal and translational-internal energy transfer terms evolution behind the shock wave: (a) ω_N RVC (solid line) and ω_N BRVC (dashed line) and (b) Ω^{TI} RVC (solid line), Ω^{CI} RVC (dashed line), Ω^{TI} BRVC (circles), and Ω^{CI} BRVC (triangles).

The analysis shown through Figs. 1–4 is restricted to a fixed number of energy bins. In order to assess the minimum number of energy bins needed to obtain an accurate description of the system dynamics, a convergence study of flow quantities has been performed. Before analyzing the results, it is worth recalling that the postshock values of pressure, temperature, and velocity for the BRVC model depend on the number of energy bins (see Table IV). The corresponding values when using the RVC model are, respectively, 11 041 Pa, 62 547 K, and 2511 m/s (not too far from those obtained with 10 and 20 energy bins).

TABLE IV. Postshock conditions (BRVC model).

N_{BP}	p_{ps} (Pa)	T_{ps} (K)	u_{ps} (m/s)
2	12 595	41 386	1457
5	11 521	56 800	2186
10	11 280	59 777	2350
20	11 151	61 302	2437
30	11 111	61 756	2464
40	11 085	62 052	2482
50	11 073	62 198	2490
75	11 060	62 336	2499
100	11 053	62 419	2504

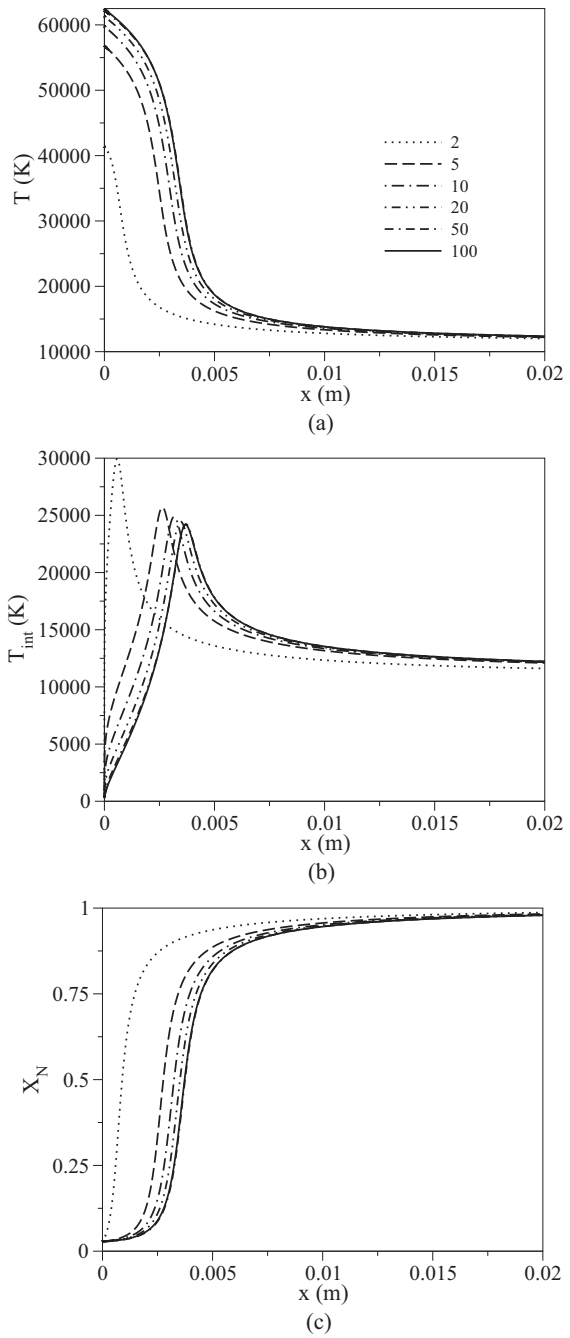

FIG. 5. Bin number convergence study of (a) the translational temperature, (b) the internal temperature, and (c) the N mole fraction evolution behind the shock wave.

Figure 5 shows the evolution of the temperatures and the N mole fraction behind the shock wave for different numbers of energy bins. The solutions obtained when using two and five energy bins overestimate the dissociation rate, implying that a larger number of bins should be used. This behavior could be partly due to the lower value of the postshock temperature. For all the cases, both the translational and internal temperature

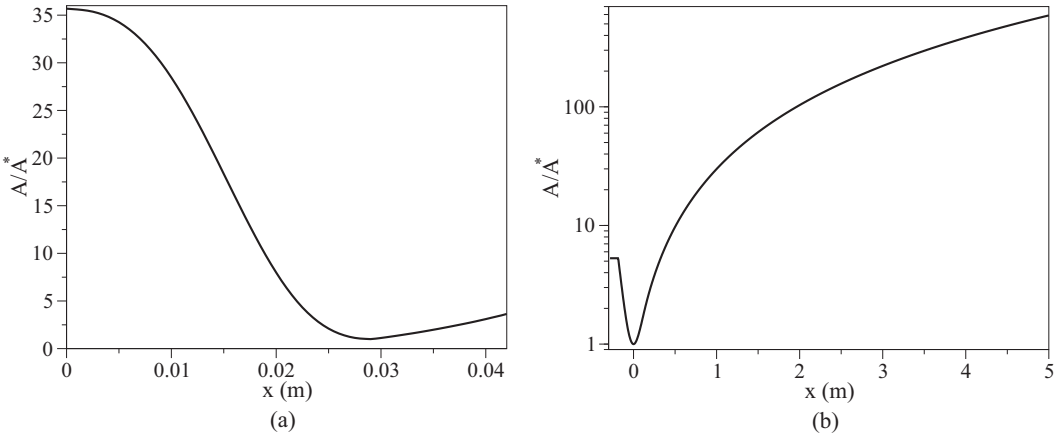

FIG. 6. Normalized area distributions of the (a) Minitorch and (b) Scirocco nozzles: (a) inlet $x = 0$ m, throat $x = 0.029$ m, and outlet $x = 0.042$ m and (b) inlet $x = -0.28$ m, throat $x = 0$ m, and outlet $x = 5$ m.

approach the postshock equilibrium value (as opposed to the case of the URVC model [49]). The dissociation dynamics is already well resolved with only 20 energy bins. The use of a larger number does not introduce appreciable changes as can be observed from the small differences between the 50- and 100-energy-bin solutions.

B. Nozzle flow

The BRVC model has been applied to study the nonequilibrium steady nozzle flow within the following realistic nozzle geometries: Minitorch (von Karman Institute) and Scirocco (Centro Italiano Ricerche Aerospaziali). Figure 6 shows their normalized area distributions.

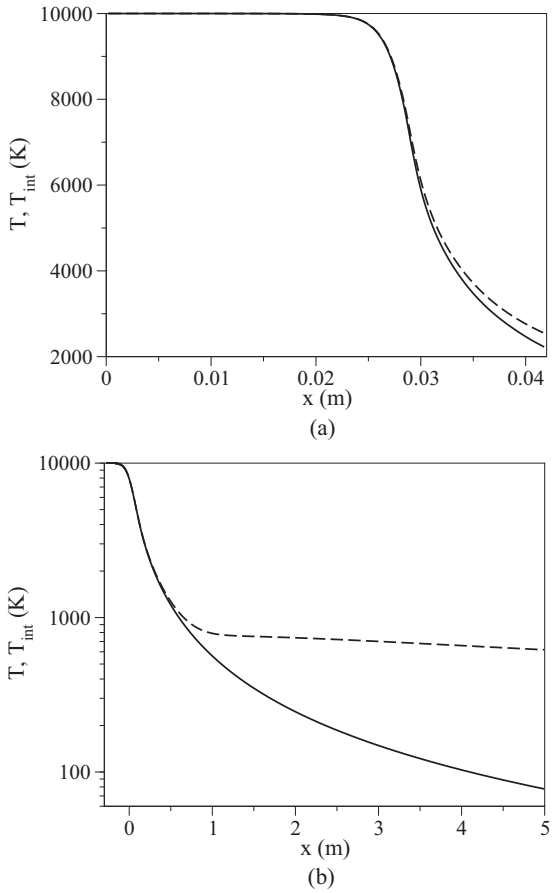

FIG. 7. Temperature evolution along the axes of the (a) Minitorch and (b) Scirocco nozzles (BRVC 100): T (solid line) and T_{int} (dashed line).

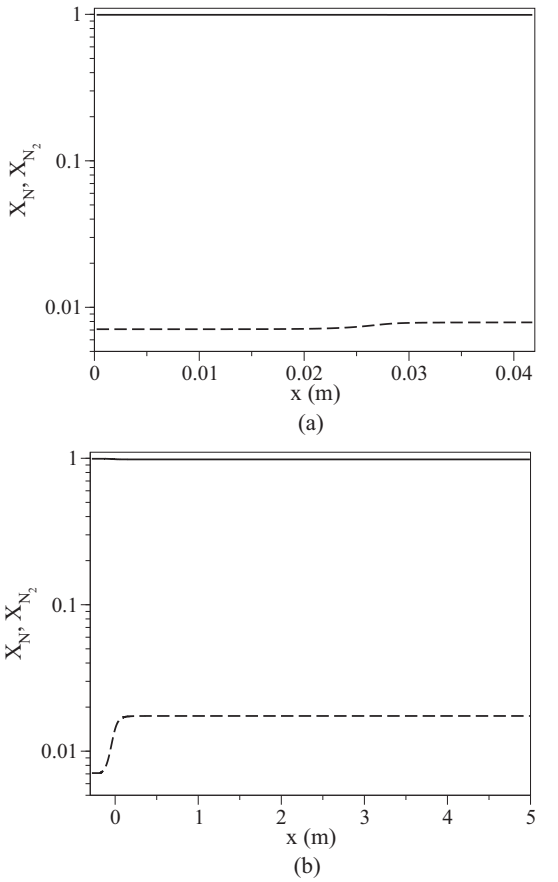

FIG. 8. Mole fraction evolution along the axes of the (a) Minitorch and (b) Scirocco nozzles (BRVC 100): X_{N} (solid line) and X_{N_2} (dashed line).

TABLE V. Nozzle outlet conditions (BRVC 100 model).

Geometry	p (Pa)	T (K)	T_{int} (K)	u (m/s)	X_{N_2}
Minitorch	2287	2225	2548	4816	7.9×10^{-3}
Scirocco	0.41	78	618	5556	1.74×10^{-2}

The calculation of the supersonic expanding flow is performed by means of the FV method discussed in Sec. III B. At the nozzle inlet, local thermodynamic equilibrium (LTE) conditions are assumed. The inlet static pressure and temperature are set to 101 325 Pa and 10 000 K, respectively. The corresponding mole fractions of N and N_2 are 0.993 and 0.07, respectively. These conditions are selected so that $N_2 + N$ collisions are the dominant mechanism in the flow.

Figures 7 and 8 show the evolution of the temperatures and the mole fractions along the nozzle axis when using 100 energy bins. The spatial evolution of the internal temperature closely follows the translational temperature. This could be due to the fact that in the definition for the internal temperature [given in Eq. (26)] rotational and vibrational levels are mixed together. The recombination occurs in correspondence with the throat region and quickly freezes [1,2] once the flow moves further downstream. The outlet conditions are provided in Table V. The expansion in the Scirocco nozzle is much more severe, as can be also inferred from Fig. 7. However, the N_2 mole fraction at the nozzle outlet is roughly twice that obtained for the Minitorch nozzle.

The dynamics of the expansion can be also investigated at the microscopic level. This is done in Fig. 9(a), showing the evolution along the axis of the Minitorch nozzle of the population distribution of the energy bins. The population is Boltzmann at the nozzle inlet, as a result of the LTE assumption. Deviations from a Boltzmann distribution occur in the throat region due to preferential recombination in high-lying energy bins. At the nozzle outlet, the distribution is highly distorted, putting forward differences in the dynamics of quasibound and bound energy bins. Figure 9(b) focuses on the population distribution at the outlet of the Minitorch nozzle. Three regions can be identified. The first comprises the energy bins close to ground state. The second includes the medium- and high-lying bound energy bins, while the third region contains all the predissociated energy bins. Temperatures are extracted for the first and third regions and are indicated in Fig. 9(b). The values obtained reveal that the bound energy bins lying close to the ground state are in partial equilibrium at the internal temperature, while the predissociated energy bins are in partial equilibrium at the translational temperature (i.e., they are in chemical equilibrium with the free state).

The computational results obtained by means of the BRVC model have been compared with the MT solution. Figure 10

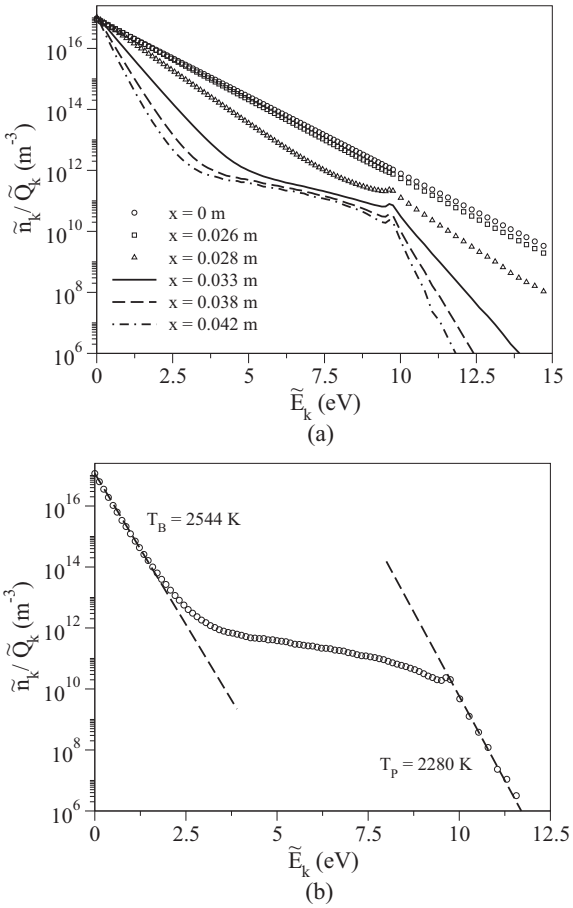

FIG. 9. Population at different locations along the axis of the Minitorch nozzle (BRVC 100): (a) evolution along the nozzle axis and (b) nozzle outlet $x = 0.042$ m.

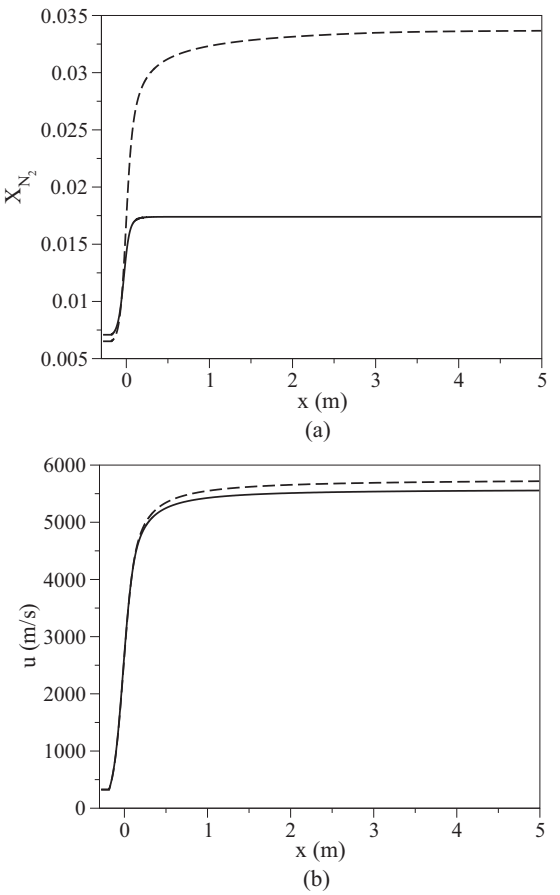

FIG. 10. Comparison between the BRVC 100 (solid line) and MT (dashed line) models for (a) the N_2 mole fraction and (b) the velocity evolution along the axis of the Scirocco nozzle.

TABLE VI. Outlet condition comparison (Scirocco nozzle).

Model	p (Pa)	T (K)	u (m/s)	X_{N_2}
BRVC 100	0.41	78	5556	1.74×10^{-2}
MT	0.67	133	5671	3.34×10^{-2}

shows a comparison for the N_2 mole fraction and the velocity in the case of the Scirocco nozzle. Outlet conditions for both models are provided in Table VI. The MT model gives almost twice the recombination predicted by the BRVC model. This in turn has an effect on the outlet values of the velocity and temperature.

A bin number convergence study has been performed for both nozzle geometries. The results for the N_2 mole fraction are shown in Fig. 11. The dynamics of recombination is already well resolved with 20 bins. Due to the limited recombination, the differences among the various solutions are less pronounced than what is observed for the flow behind a normal shock wave (see Fig. 5). The same holds true for flow quantities such as velocity and temperatures (not shown here).

The influence of the number of energy bins can also be observed at the microscopic level, as done in Fig. 12, showing the population distribution at the outlet of the Minitorch nozzle for different numbers of energy bins.

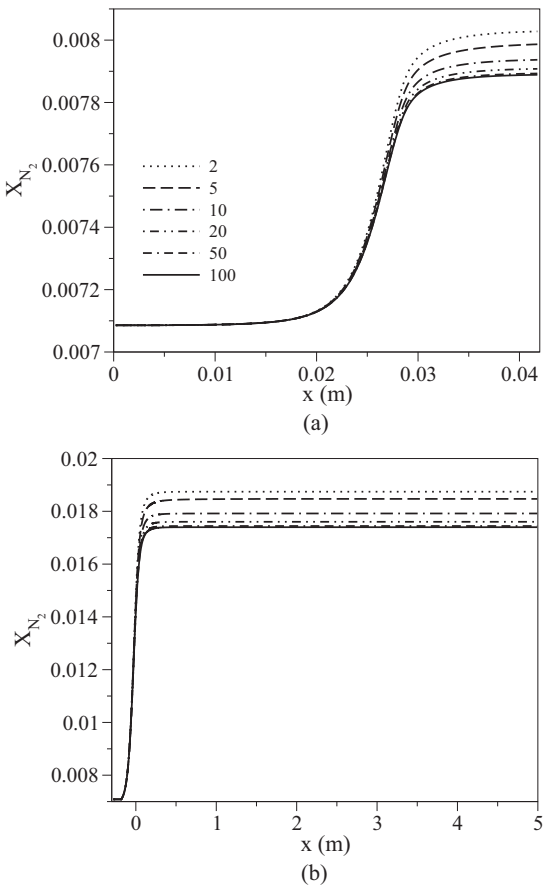

FIG. 11. Bin convergence study of the N_2 mole fraction evolution along the axes of the (a) Minitorch and (b) Scirocco nozzles.

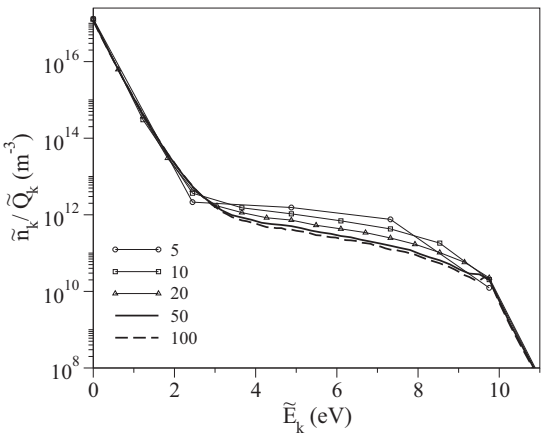

FIG. 12. Bin convergence study of the outlet population for the Minitorch nozzle.

V. CONCLUSION

A Boltzmann rovibrational collisional coarse-grained model for internal energy excitation and dissociation in hypersonic flows has been proposed as alternative to a previously developed uniform coarse-grained model. The model has been built by lumping the rovibrational energy levels of the N_2 molecule into energy bins and by assuming that the levels within each bin are populated according to a Boltzmann distribution at the local translational temperature. Rate coefficients for collisional excitation and dissociation have been obtained by averaging the elementary rovibrational kinetic data provided by the Computational Quantum Chemistry Group at NASA Ames Research Center.

Applications have focused on the investigation of the nonequilibrium flows behind a normal shock wave and inside two different nozzles. The computational results obtained have shown that the proposed coarse-grained model is able to provide an accurate description of the dynamics of internal energy excitation and dissociation with only 20 energy bins. Excellent agreement with the numerical solutions obtained by direct solution of the master equation of the rovibrational collisional model has been observed.

Future work would entail the extension of the model to dissipative transport. The flow governing equations and the expressions of the transport fluxes can be obtained based on the kinetic theory of gases. A complete derivation was performed for vibrational collisional models in Ref. [58] and preliminary results were obtained for a model similar to the bin approach in Ref. [69]. In this situation, a difficulty is the identification of the collision invariants of the fast collision operator requiring an expansion in the perturbation parameters [58,69].

ACKNOWLEDGMENTS

The authors have benefited from numerous discussions with Dr. R. L. Jaffe, Dr. D. W. Schwenke, Dr. G. Chaban, Dr. W. Huo, and Dr. Y. Liu at NASA Ames Research Center. We gratefully acknowledge Dr. A. Bourdon at the EM2C Laboratory for help with processing the kinetic database.

The research of A.M. and T.E.M. was sponsored by the European Research Council Starting Grant No. 259354. The research of M.P. was sponsored by the University of Illinois at Urbana-Champaign Starting Grant.

[1] C. Park, *Nonequilibrium Hypersonic Aerothermodynamics* (Wiley, New York, 1990).
[2] W. G. Vincenti and C. H. Kruger, *Introduction to Physical Gas Dynamics* (Wiley, New York, 1965).
[3] P. A. Gnoffo, Annu. Rev. Fluid Mech. **31**, 459 (1999).
[4] L. C. Woods, *The Thermodynamics of Fluid Systems* (Clarendon, Oxford, 1975).
[5] J. H. Ferziger and H. G. Kaper, *Mathematical Theory of Transport Processes in Gases* (North-Holland, Amsterdam, 1972).
[6] G. A. Bird, *Molecular Gas Dynamics and the Direct Simulation of Gas Flows* (Clarendon, Oxford, 1994).
[7] T. E. Magin and G. Degrez, Phys. Rev. E **70**, 046412 (2004).
[8] E. V. Kustova and L. A. Puzyreva, Phys. Rev. E **80**, 046407 (2009).
[9] M. Capitelli, R. Celiberto, C. Gorse, A. Laricchiuta, D. Pagano, and P. Traversa, Phys. Rev. E **69**, 026412 (2004).
[10] S. Pascal and R. Brun, Phys. Rev. E **47**, 3251 (1993).
[11] M. Panesi, T. E. Magin, A. Bourdon, A. Bultel, and O. Chazot, J. Thermophys. Heat Transfer **23**, 236 (2009).
[12] M. Panesi, T. E. Magin, A. Bourdon, A. Bultel, and O. Chazot, J. Thermophys. Heat Transfer **25**, 361 (2011).
[13] A. Aliat, A. Chikhaoui, and E. V. Kustova, Phys. Rev. E **68**, 056306 (2003).
[14] A. Munafò, M. Panesi, R. L. Jaffe, G. Colonna, A. Bourdon, and T. E. Magin, Eur. Phys. J. D **66**, 188 (2012).
[15] G. Colonna and M. Capitelli, J. Thermophys. Heat Transfer **15**, 308 (2001).
[16] C. Park, J. Thermophys. Heat Transfer **9**, 17 (1995).
[17] V. Babu and V. V. Subramaniam, J. Thermophys. Heat Transfer **9**, 227 (1995).
[18] M. Panesi, R. L. Jaffe, D. W. Schwenke, and T. E. Magin, J. Chem. Phys. **138**, 044312 (2013).
[19] C. Park, J. Thermophys. Heat Transfer **7**, 385 (1993).
[20] C. Park, R. L. Jaffe, and H. Partridge, J. Thermophys. Heat Transfer **15**, 76 (2001).
[21] G. V. Candler and R. W. MacCormack, J. Thermophys. Heat Transfer **5**, 266 (1991).
[22] P. A. Gnoffo, R. N. Gupta, and J. L. Shinn, NASA Technical Report No. 2867, 1989.
[23] A. Lani, M. Panesi, and H. Deconinck, Commun. Comput. Phys. **13**, 479 (2013).
[24] C. Park, *Proceedings of the 48th AIAA Aerospace Sciences Meeting including the New Horizons Forum and Aerospace Exposition, Orlando*, *AIAA paper 2010-0911* (AIAA, Reston, VA, 2010).
[25] R. L. Jaffe, D. W. Schwenke, G. Chaban, and W. Huo, *Proceedings of the 46th AIAA Aerospace Sciences Meeting and Exhibit, Reno, AIAA paper 2008-1208* (AIAA, Reston, VA, 2008).
[26] R. L. Jaffe, D. W. Schwenke, and G. Chaban, *Proceedings of the 47th AIAA Aerospace Sciences Meeting including the New Horizons Forum and Aerospace Exposition, Orlando*, *AIAA paper 2009-1569* (AIAA, Reston, VA, 2009).
[27] G. Chaban, R. L. Jaffe, D. W. Schwenke, and W. Huo, *Proceedings of the 46th AIAA Aerospace Sciences Meeting and Exhibit, Reno, AIAA paper 2008-1209* (Ref. [25]).
[28] F. Esposito and M. Capitelli, Chem. Phys. Lett. **302**, 49 (1999).
[29] F. Esposito and M. Capitelli, Chem. Phys. **257**, 193 (2000).
[30] F. Esposito, I. Armenise, and M. Capitelli, Chem. Phys. **331**, 1 (2006).
[31] I. Armenise, M. Capitelli, R. Celiberto, G. Colonna, C. Gorse, and A. Lagana, Chem. Phys. Lett. **227**, 157 (1994).
[32] M. Capitelli, I. Armenise, D. Bruno, M. Cacciatore, R. Celiberto, G. Colonna, O. D. Pascale, P. Diomede, F. Esposito, C. Gorse, K. Hassouni, A. Laricchiuta, S. Longo, D. Pagano, D. Pietanza, and M. Rutigliano, Plasma Sources Sci. Technol. **16**, S30 (2007).
[33] J. G. Kim, O. J. Kwon, and C. Park, J. Thermophys. Heat Transfer **23**, 443 (2009).
[34] A. Bultel, B. van Ootegem, A. Bourdon, and P. Vervisch, Phys. Rev. E **65**, 046406 (2002).
[35] A. Bultel, B. G. Chéron, A. Bourdon, O. Motapon, and I. F. Schneider, Phys. Plasmas **13**, 043502 (2006).
[36] A. Bourdon and P. Vervisch, Phys. Rev. E **54**, 1888 (1996).
[37] A. Bourdon, Y. Térésiak, and P. Vervisch, Phys. Rev. E **57**, 4684 (1998).
[38] S. T. Surzhikov, J. Heat Transfer **134**, 031002 (2012).
[39] J.-L. Cambier and S. Moreau, *Proceedings of the 24th AIAA Plasmadynamics and Laser Conference, Orlando, AIAA paper 1993-3196* (AIAA, Reston, VA, 1993).
[40] A. Aliat, P. Vedula, and E. Josyula, Phys. Rev. E **83**, 067302 (2011).
[41] E. V. Kustova, Chem. Phys. **270**, 177 (2001).
[42] M. G. Kapper and J.-L. Cambier, J. Appl. Phys. **109**, 113308 (2011).
[43] M. G. Kapper and J.-L. Cambier, J. Appl. Phys. **109**, 113309 (2011).
[44] A. Munafò, M. G. Kapper, J.-L. Cambier, and T. E. Magin, *Proceedings of the 50h AIAA Aerospace Sciences Meeting including the New Horizons Forum and Aerospace Exposition, Nashville, AIAA paper 2012-0647* (AIAA, Reston, VA, 2012).
[45] G. V. Candler, J. Olejniczak, and B. Harrold, Phys. Fluids **9**, 2108 (1997).
[46] E. Josyula and W. F. Bailey, J. Thermophys. Heat Transfer **15**, 157 (2001).
[47] E. Josyula, W. F. Bailey, and S. M. Ruffin, Phys. Fluids **15**, 3223 (2003).
[48] G. Colonna, I. Armenise, D. Bruno, and M. Capitelli, J. Thermophys. Heat Transfer **20**, 477 (2006).
[49] T. E. Magin, M. Panesi, A. Bourdon, R. L. Jaffe, and D. W. Schwenke, Chem. Phys. **398**, 90 (2012).
[50] M. Panesi and A. Lani, Phys. Fluids **25**, 057101 (2013).
[51] Y. Liu, M. Panesi, M. Vinokur, and P. Clarke, *Proceedings of the 44th AIAA Thermophysics Conference, San Diego*, *AIAA paper 2013-3146* (AIAA, Reston, VA, 2013).
[52] A. Guy, A. Bourdon, and M. Y. Perrin, Chem. Phys. **420**, 15 (2013).

[53] P. L. Varghese and D. A. Gonzales, in *Molecular Physics and Hypersonic Flows*, edited by M. Capitelli, NATO Advanced Studies Institute Series (Kluwer Academic Publishers, Dordrecht, 1996), Vol. 482, pp. 105–114.

[54] M. Panesi, R. L. Jaffe, and D. W. Schwenke, *Proceedings of the 44th AIAA Thermophysics Conference, San Diego*, *AIAA paper 2013-3147* (Ref. [51]).

[55] D. W. Schwenke, J. Chem. Phys. **89**, 2076 (1988).

[56] R. J. Le Roy, Y. Huang, and C. Jary, J. Chem. Phys. **125**, 164310 (2006).

[57] V. Giovangigli, *Multicomponent Flow Modeling* (Birkhäuser, Boston, 1999).

[58] E. Nagnibeda and E. Kustova, *Non-Equilibrium Reacting Gas Flows* (Springer, Berlin, 2009).

[59] M. Panesi, A. Munafò, R. L. Jaffe, and T. E. Magin (unpublished).

[60] C. Hirsch, *Numerical Computation of Internal and External Flows* (Wiley, New York, 1990).

[61] C. W. Gear, *Numerical Initial-Value Problems in Ordinary Differential Equations* (Prentice-Hall, Englewood Cliffs, NJ, 1971).

[62] K. Radhakrishnan and A. C. Hindmarsh, NASA Report No. 1327, 1993.

[63] P. L. Roe, J. Comput. Phys. **43**, 357 (1981).

[64] R. K. Prabhu, NASA Report No. 194867, 1994.

[65] M.-S. Liou and B. van Leer, *Proceedings of the 26th AIAA Aerospace Sciences Meeting, Reno*, *AIAA paper 1988-0624* (AIAA, Reston, VA, 1988).

[66] B. van Leer, J. Comput. Phys. **32**, 101 (1979).

[67] G. D. van Albada, B. van Leer, and W. W. Roberts, Jr., Astron. Astrophys. **108**, 76 (1982).

[68] J. G. Parker, Phys. Fluids **2**, 449 (1959).

[69] T. E. Magin, M. Massot, and B. Graille, in *Proceedings of the 28th International Symposium on Rarefied Gas Dynamics*, edited by M. Mareschal and A. Santos, AIP Conf. Proc. No. 1501 (AIP, New York, 2012).